

Crystallization and topology-induced dynamical heterogeneities in soft granular clusters

Michał Bogdan^{1,*}, Jesus Pineda^{2,†}, Mihir Durve,³ Leon Jurkiewicz,¹ Sauro Succi,^{3,4,5}
Giovanni Volpe^{2,‡} and Jan Guzowski^{1,§}

¹*Institute of Physical Chemistry, Polish Academy of Sciences, Kasprzaka 44/52, 01-224 Warsaw, Poland*

²*Department of Physics, University of Gothenburg, Origovägen 6 b 41296 Göteborg, Sweden*

³*Center for Life Nano- & Neuro-Science, Fondazione Istituto Italiano di Tecnologia (IIT), viale Regina Elena 295, 00161 Rome, Italy*

⁴*Istituto per le Applicazioni del Calcolo del Consiglio Nazionale delle Ricerche, via dei Taurini 19, 00185 Rome, Italy*

⁵*Department of Physics, Harvard University, 17 Oxford Street, Cambridge, Massachusetts 02138, USA*



(Received 25 April 2023; accepted 6 June 2024; published 8 August 2024)

Soft-granular media, such as dense emulsions, foams or tissues, exhibit either fluid- or solidlike properties depending on the applied external stresses. Whereas bulk rheology of such materials has been thoroughly investigated, the internal structural mechanics of finite soft-granular structures with free interfaces is still poorly understood. Here, we report the spontaneous crystallization and melting inside a model soft granular cluster—a densely packed aggregate of $N \sim 30$ –40 droplets engulfed by a fluid film—subject to a varying external flow. We develop machine learning tools to track the internal rearrangements in the quasi-two-dimensional cluster as it transits a sequence of constrictions. As the cluster relaxes from a state of strong mechanical deformations, we find differences in the dynamics of the grains within the interior of the cluster and those at its rim, with the latter experiencing larger deformations and less frequent rearrangements, effectively acting as an elastic membrane around a fluidlike core. We conclude that the observed structural-dynamical heterogeneity results from an interplay of the topological constraints, due to the presence of a closed interface, and the internal solid-fluid transitions. We discuss the universality of such behavior in various types of finite soft granular structures, including biological tissues.

DOI: [10.1103/PhysRevResearch.6.L032031](https://doi.org/10.1103/PhysRevResearch.6.L032031)

Soft granular materials, such as dense foams, emulsions and biological tissues, consist of densely-packed deformable grains, separated by a thin layer of a lubricating fluid [1–7]. Complex behaviors, like memory effects, avalanches, plasticity, and viscoelasticity, emerge from multiscale interactions in these systems [8–14]. Despite advances in soft glass theories of bulk materials [15], the structural mechanics and microrheology of finite-sized soft granular clusters remain poorly understood. Examples of such clusters include cell aggregates like embryos [16,17], circulating tumor cell clusters [18], cell spheroids used in biomimetic experiments [19] and droplet/bubble clusters or jets used as templates in fabrication of porous materials [20,21].

Freely-floating small soft-granular clusters, with droplets playing the role of grains, have been previously assembled using microfluidics [22–26]. However, while very small close-packed clusters (typically $N < 10$ droplets) formed by the inner droplets in a larger double emulsion drop have been

thoroughly studied in terms of their equilibrium stable and metastable morphologies [24,27,28], little is known about the complex internal dynamics of mesoscale clusters, including their microrheology and internal solid-fluid transitions in response to external stresses or upon relaxation.

Recent microfluidic experiments involving aggregates of living cells or synthetic biomimetic prototissues ($N \sim 10^2$ cells) have revealed intriguing relaxation dynamics [19,29]. However, the challenges associated with cell polydispersity and heterogeneous interactions limited the control over the system at the microscale. Here, we propose a convenient model system: a double emulsion drop encapsulating multiple close-packed and highly monodisperse inner droplets, all confined in a shallow microchannel. The system allows us to control generation and manipulation of the droplet clusters as well as to precisely track the internal droplet rearrangements under external microflows.

It is known that monodisperse two-dimensional (2D) systems feature crystallization, understood here as ordering into a 2D Bravais lattice, usually a hexagonal one. However, so far, crystallization has been experimentally observed only in very large systems, and in systems confined by rigid walls [30–36]. While some limited numerical work on the structural dynamics of freely floating droplet clusters has been previously reported [14,37], the actual order-disorder transitions in such systems have not been investigated.

Here, we use a microfluidic system (see Fig. 1) which enables sequential generation and manipulation of granular clusters using external flows under quasi-2D confinement. We

*Contact author: mbogdan@ichf.edu.pl

†Contact author: jesus.pineda@physics.gu.se

‡Contact author: giovanni.volpe@physics.gu.se

§Contact author: jguzowski@ichf.edu.pl

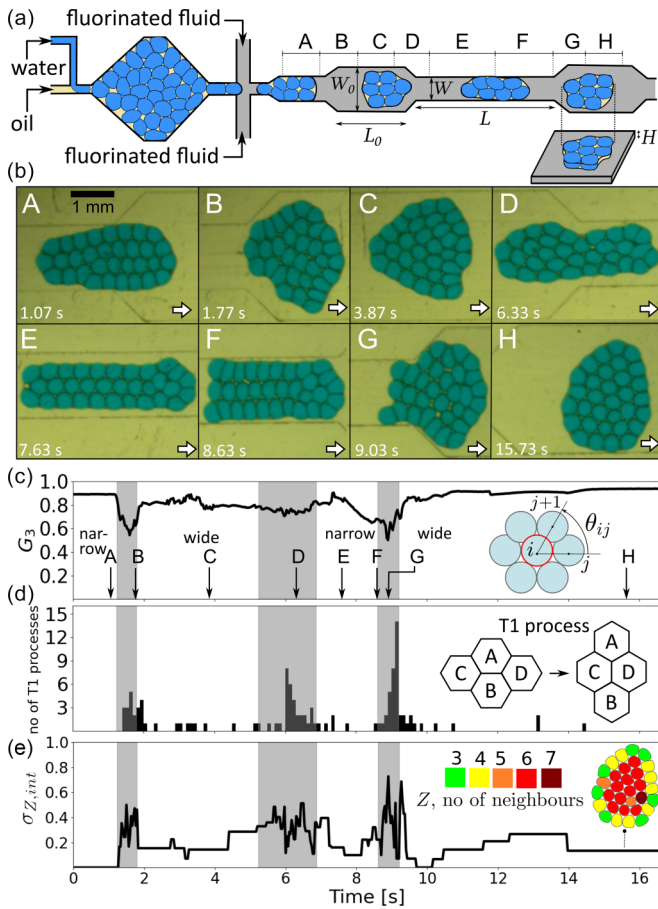


FIG. 1. (a) Scheme of the microfluidic system for the production of clusters of a soft granular medium. $L = 10$ mm, $L_0 = 5$ mm, $W = 1.4$ mm, $W_0 = 2.8$ mm, $H = 0.25$ mm. (b) Snapshots of the cluster at different times corresponding to different sections of the channel, A–H (see also Supplemental Material movie SM1 [38]). (c) Order parameter G_3 (see main text) of the cluster as a function of time. Gray areas corresponds to the sections of changing width, white areas correspond to constant width. (d) The number of T1 processes in 0.1 s intervals. (e) The variance $\sigma_{Z,int}$ of the number of nearest neighbors for droplets in the interior of the cluster. The inset displays the color-coded numbers of nearest neighbors for each droplet in the cluster at late times.

precisely control the flow of the external carrier fluid to push the clusters via a sequence of constrictions and track the internal dynamics upon flow-induced deformation and subsequent relaxation.

Our methods are partially based on our previous work, wherein we investigated the stochastic jetting-dripping transition of a close-packed emulsion subject to flow-focusing by an external immiscible phase [39]. Here, using a modified experimental setup, we focus strictly on the internal dynamics of the clusters, typically consisting of $N \sim 20$ –40 droplets. In particular, we observe spontaneously emerging structural-dynamical heterogeneity between two droplet subpopulations: those at the rim of the cluster and those in the interior. To reveal such spontaneous structural segregation we develop a machine-learning-based method of droplet segmentation and tracking based on the DeepTrack-2 framework [40] (see

Supplemental Material [38]). We analyze multiple recorded videos frame-by-frame to find that the droplets at the rim get systematically more strongly deformed and rearrange less frequently in response to external flow-induced stresses. Accordingly, we find that the clusters spontaneously develop an internal mesostructure consisting of an elastic granular membrane around a more fluid-like granular core.

Finally, we also find that sufficiently strong deformations of the cluster, as it transits the constrictions under flow, may eventually force the droplets from the core to enter the rim. This results in effective mixing between the cluster’s two subpopulations, which could have applications, e.g., in microfluidics-assisted microtissue engineering.

Our double-emulsion system consists of densely packed blue-dyed aqueous droplets encapsulated by a thin film of oil with surfactant (see Supplemental Material (SM) [38]). The droplets are created at a T junction and fed to a chamber [see Fig. 1(a) and SM0 [38]]. From there, the desired volume of the monodisperse emulsion (dictated by the intended size of the cluster) is pushed out into a narrow channel, where, at a cross junction, it is cut by a third immiscible phase, a fluorinated liquid. Since the droplets are spontaneously engulfed by the oil phase due to preferential wetting [41], we observe the formation of a double-emulsion cluster containing multiple aqueous cores (droplets) inside a thin oil shell carried by the flow of the external fluorinated fluid. The cluster is subsequently pushed through a sequence of widenings and narrowings [see Fig. 1(a)]. We observe the patterns of droplet rearrangements within the cluster upon its compression and relaxation. The velocity of the cluster is regulated by the applied rate of flow of the external fluorinated phase. We choose a representative cluster ($N = 32$, movie SM1 [38].) to illustrate a collection of phenomena observed widely throughout the experiments [38].

We observe crystallization of droplets into a near-hexagonal lattice in the wide fragments of the channel when the clusters move at a constant velocity. The evolution of the cluster in Fig. 1(b) under an external flow rate of 8 ml/h illustrates this phenomenon. To quantify the level of droplet ordering we analyze the cluster-averaged orientational order parameter G_3 [42] defined for each droplet i as $G_{3,i} = \frac{1}{N_i} \sum_{j=1}^{N_i} |\cos(3\theta_{ij})|$, where N_i is the number of neighbors of the droplet i and θ_{ij} is the bond angle centered at droplet i with arms pointing to the centers of two droplets neighboring droplet i and each other [j labels such pairs, see the inset in Fig. 1(c)]. G_3 is known to be the measure of hexagonal order [42], in particular, $G_3 = 1$ for a perfect hexagonal lattice [Fig. 1(c)]. We also observe that the local arrangements of droplets during transfer through the wider sections remain mostly unchanged, with only individual T1 processes [43] [i.e., swapping of neighbors between droplets; see the inset in Fig. 1(d) for illustration]. Note that apart from a classical swapping of neighbours between four droplets [as shown in the inset in Fig. 1(d)], we also consider a T1 process a rearrangement in which a droplet enters or leaves the rim, therefore affecting the order of droplets in the rim. Later in the text we refer to the former type of rearrangement as a T1 process in the interior and to the latter as a T1 process in the rim. As the cluster enters a widening or narrowing [see Figs. 1(b) and 1(c)], we observe a rheological solid-fluid transition. This is signified by the increased frequency of T1

processes occurring in parallel with the change of the shape of the cluster. We refer to this process as melting. The internal hexagonal structure is destroyed and G_3 correspondingly decreases.

The cycles of crystallization and melting can be also seen in the variance $\sigma_{Z,\text{int}}$ of the number Z of neighbors of droplets within the interior of the cluster [Fig. 1(e)], where, as expected for a monodisperse system, $\text{median}(Z) = 6$. We find that $\sigma_{Z,\text{int}}$ is relatively low in channel sections of a constant width, or in the absence of flow, and increases when the cluster transits a constriction. In the final relaxed state, we find one positive and seven negative defects in the rim (defined as the droplets directly touching the interface of the emulsion with the external fluid) and 1 positive and 1 negative topological defect in the interior (the remaining droplets). This configuration closely resembles the energy-minimizing cluster ($N = 32$) predicted numerically by Cox *et al.* [44]. We conclude that the observed cluster relaxes to a final state which is very close to the actual global energy minimum.

Overall, we find that the extensional or compressional flows, experienced by a cluster upon entering or exiting a constriction, increase the level of fluidity in the system. This can be also analyzed based on the patterns of droplet motion in the center-of-mass reference frame [38].

We note that a flow of 8 mL/h (as in SM1 [38]) implies a capillary number $\text{Ca} \equiv \eta U / \gamma \approx 0.37 \times 10^{-2}$ and $\text{Ca} \approx 0.74 \times 10^{-2}$ within the wide and narrow channel, respectively, where η is the viscosity of the oil, γ is the interfacial tension between the water and oil phases and U is the velocity of the fluids, averaged over the channel cross section. We note that this is close to the values of Ca at which a crossover between fluidlike and solidlike patterns of motion have been reported for a monodisperse quasi-2D dense emulsion [45].

One of our most intriguing findings is that the process of melting, understood as the intensification of T1 processes, occurs mostly in the interior of the cluster, while the rim of the cluster responds more as an elastic solid, absorbing stresses via droplet deformations (see Figs. 2(a) and 2(b) and SM [38]). In particular, we observe that, upon exiting a constriction, the droplets in both interior and rim undergo fast, externally enforced shape deformations, and develop a temporary compression front which gradually dissolves as the droplets in the interior start to rearrange undergoing numerous T1 processes and quickly regaining their average circularity $C \equiv 4\pi A / P^2$, where P is the perimeter and A is the area of a droplet (note $4\pi A / P^2 = 1$ for a perfect circle). In contrast, the droplets in the rim feature fewer T1 processes and recover their circular shape much more slowly. Quantitatively, during the relaxation stage (see $t \in [1.36, 4.13]$ s and $[8.85, 15.73]$ s), whose onset is defined as the point when C of the interior droplet population reaches a minimum, we observe around five times less rearrangements at the rim than in the interior of the cluster. Based on six relaxation events and 149 T1 processes in movies SM1, SM2, SM3, SM4 and SM5 [38], we obtain an average 0.31 T1 processes per droplet in the rim and an average 1.52 T1 processes per droplet in the interior per relaxation event. We suspect that this dynamic segregation effect results from stronger confinement of the droplets at the rim and their resultant inability to release mechanical frustrations.

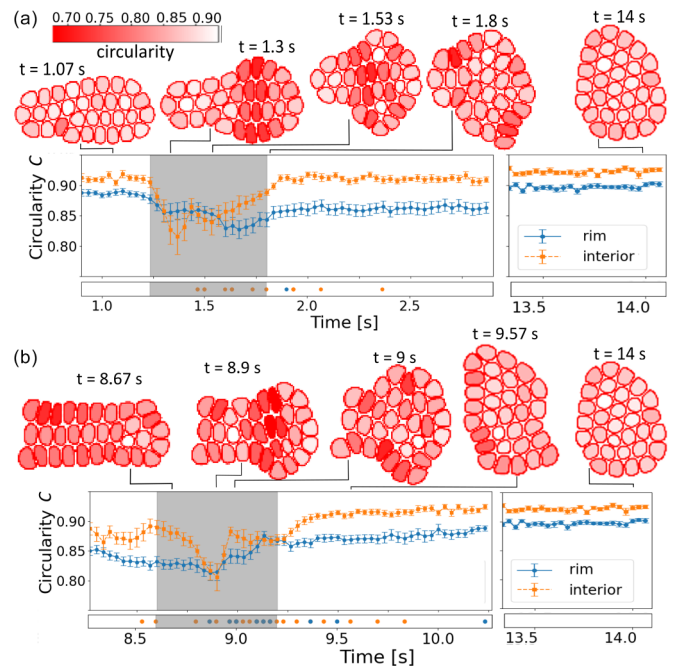


FIG. 2. (a) Circularity of the droplets $C \equiv 4\pi A / P^2$, where P is the perimeter and A the area of a droplet (note $4\pi A / P^2 = 1$ for a perfect circle), in the rim and interior subpopulations as a function of time for the first relaxation event [sections A–C of the channel, see Fig. 1(a)]. The color-coded snapshots display the spatial variations in the droplet circularity (red-lowest, white-highest) within the cluster at different time points. The separate plot and snapshot on the right indicate the close-to-equilibrium configuration at late times. The occurrence of T1 processes in the rim (blue) and interior (orange) of the cluster (see the main text for a precise definition) is indicated as a point process in time beneath the main plot. (b) Data analogous to (a) for the second relaxation event (sections F–H). Error bars indicate the standard errors of the mean.

We note that the expected *equilibrium* circularity values for the interior and the rim populations are actually slightly different due to the slightly different droplet shapes in the corresponding inner and outer regions of the cluster. This can be seen in Fig. 2, where the initial and late-time values of C —which may be considered very close to the global equilibrium—differ by around 3% for the two populations. In fact, the droplets at the rim remain slightly more deformed than in the interior. The difference may seem minor, however, it is comparable with the dynamic variations in the circularities during the relaxation process, the latter not exceeding around 10%. Therefore, in order to properly visualize the relaxation dynamics for the two droplet populations, in Figs. 3(a) and 3(b) we replot the respective circularities shifted with respect to the minimum value and normalized to the overall amplitude, i.e., we plot $C^*(t) = (C(t) - C_{\min}) / (C_{\max} - C_{\min})$. Note that C_{\min} is taken as the minimum of $C(t)$ over the chosen relaxation event while C_{\max} is taken as the maximum of $C(t)$ over the whole experiment (not only the relaxation phase). With such a choice, C_{\max} serves as the best approximation of the actual equilibrium. The rescaled plots in Fig. 3 directly demonstrate the effect of the *dynamic* heterogeneity of the cluster, i.e., with subtracted effects of the *static*

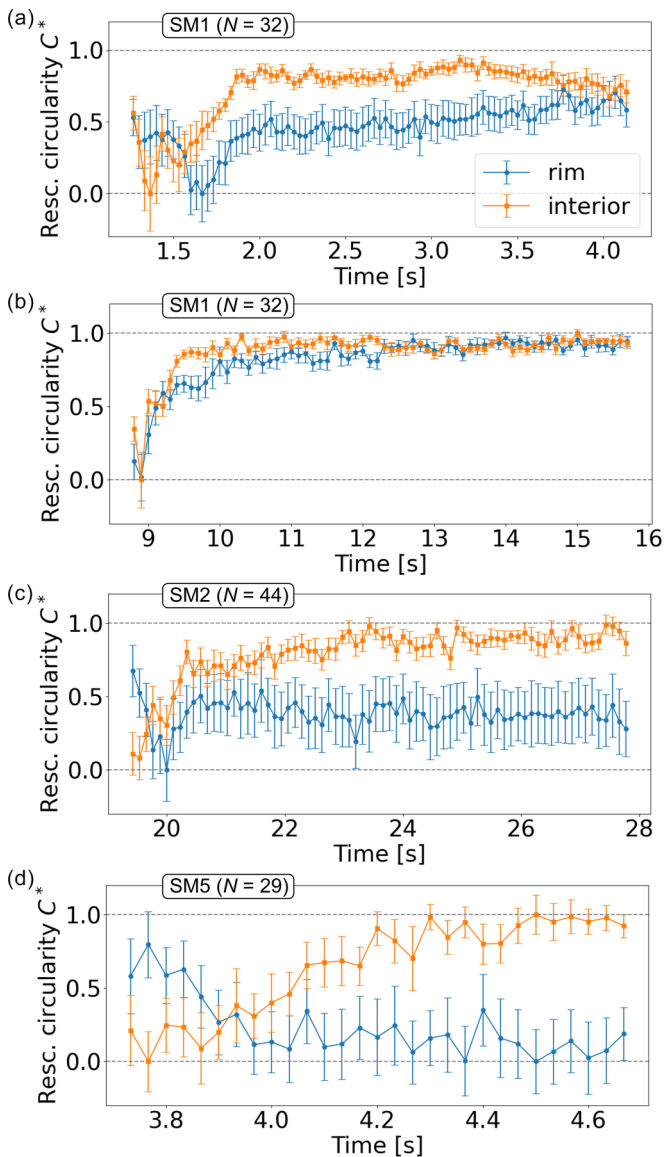


FIG. 3. Rescaled circularity of the droplets defined as $C^*(t) \equiv (C(t) - C_{\min}) / (C_{\max} - C_{\min})$ in the rim and interior populations during the relaxation phase for three different clusters (from top to bottom respectively clusters in supporting movies SM1, SM1, SM2, SM5 [38]). (a) and (b) correspond to different compression events for the same cluster. Error bars indicate the standard errors of the mean. (c) and (d) compression events in different clusters.

(equilibrium) heterogeneity. The effect of the dynamic segregation is clearly reproducible for sufficiently large clusters [$N \sim 30-40$; see Figs. 3(c) and 3(d)]. For smaller clusters ($N \sim 20$) we observe more stochastic behavior and less (or none) segregation effects (see Figs. S3(c), S3(d), and S5 [38]).

In the case of the larger clusters, in three out of four considered relaxation events [Figs. 3(a), 3(c) and 3(d)], we also find that the interior population experiences the maximal reduction of circularity before the rim population. This characteristic phase-shift in the early stages of the relaxation period signifies that the rapid fluidization of the interior accompanies initial solidlike deformation of the rim. At later stages, in all cases [Figs. 3(a)–3(d)], the rim population recovers its

circularity much slower than the interior. Note that in the event presented in Fig. 3(d), due to the short observation window, the rim population remains close to the maximally distorted state up to the end of the plotted period, while the interior quickly relaxes and reaches the maximum circularity. Note also that for clarity in Figs. 3(a) and 3(b) we have plotted $C^*(t)$ for every third and every second frame, respectively.

The data presented in Figs. 2 and 3 provide evidence that the relaxing clusters under moderate perturbations develop a fluidized core surrounded by an elastic membrane. The effect is apparently mainly of topological origin. We propose that this dynamic segregation occurs because the shape of the cluster is changed by the external flow at a time scale τ_{flow} which is shorter than or comparable to the time scale τ_{T1} needed for a T1 process to occur. To check this hypothesis, we measure τ_{T1} during periods when the cluster is flowing in the wider chamber without extensional strains ($t \in [2.53, 4.90]$ s in SM1 [38]). Based on averaging over six T1 processes we obtain $\tau_{T1} = 0.56$ s. We also estimate $\tau_{\text{flow}} \approx l / (U - U_0)$, where $U = Q / (HW)$, $U_0 = Q / (HW_0)$ are the average velocities of the flow in the narrower and wider sections of the channel, respectively, and $l = 0.7$ mm is the length over which the width of the channel is changing. We find $\tau_{\text{flow}} = 0.22$ s, such that $\tau_{\text{flow}} \lesssim \tau_{T1}$, in agreement with the expectations. We also note that, for the segregation effect to be observable, the time scale of the experiment τ_{exp} must also be much longer than τ_{T1} . Accordingly, the general condition can be formulated as $\tau_{\text{flow}} \lesssim \tau_{T1} \ll \tau_{\text{exp}}$. It is obeyed in our case, since $\tau_{\text{exp}} \approx 13$ s and $\tau_{\text{exp}} \in [4, 15]$ s in the other experimental runs.

In general, the arrest of the droplets at the rim could be caused not only by the topology, i.e., the closed interface, but also by direct interaction of the droplets with the interface, e.g., due to the partial wetting of the droplets by the external, fluorinated phase. In our case, however, the three-phase (water-oil-external) contact angle appears to be too small to be measured directly, from which we conclude that the adhesion is likely negligible. Accordingly, we argue that the arrest of the droplets at the interface is mainly of topological origin whereas the interface effectively reduces the number of degrees of freedom and prevents, or significantly slows down, the rearrangements. Nevertheless, in general, the prevalence and relative importance of either the topological arrest or direct adhesion to the interface would depend on the actual experimental conditions, e.g., the precise chemical compositions of the external phase and the middle oil phase.

We also find that, in spite of the enhanced arrest of the droplets at the rim during the relaxation events, sufficiently strong deformations of the cluster upon transiting the subsequent constrictions can be used to impose gradual mixing of the rim and interior subpopulations (Fig. 4). In fact, we find that as the cluster exits the first constriction, it rounds up and reduces its perimeter [Fig. 4(a), $t = 3.87$ s], so that eventually some droplets from the frontal, downstream section of the rim enter the core. Subsequently, as the cluster enters the second constriction [Fig. 4(b)], the frontal part is again rolled up forcing even more droplets from the rim into the interior. Later in the constriction, as the cluster unfolds into a 3-row plug ($t = 7.63$ s) and increases its perimeter, the droplets from the interior enter the rim, whereas upon exiting the constriction [Fig. 4(c)] we observe an opposite process. Overall,

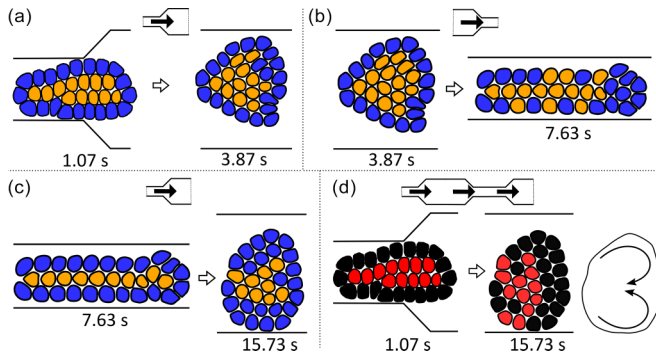


FIG. 4. Mixing of droplets forming the initial rim (blue) and interior subpopulations (yellow), separately for each of the three translocations: (a) first widening, (b) narrowing, (c) second widening. (d) Cumulative process for the entire sequence, with initial rim and interior droplets colored black and red, respectively. The scheme on the right indicates the direction of effective recirculation.

however, there is no reversibility in the droplet rearrangements [Fig. 4(d)] and we observe gradual mixing within the cluster. The process apparently involves shifting of the droplets from the front to the back of the cluster, thus resembling internal recirculation in a simple viscous plug [46], however, with the opposite direction of the recirculation.

In summary, we report the microrheology and internal structural transitions within soft granular clusters modeled by a double-emulsion drop with multiple close-packed inner droplets. We find that in the midsize clusters ($N \sim 30-40$) the subpopulations of the droplets within the interior and at the rim of the cluster develop different mechanical responses to the external stresses, with the rim acting effectively as an elastic membrane around a more fluidlike core, an effect which we attribute to the topology of the system itself (a closed interface).

Due to the topological nature of this effect, it could be present in a wide spectrum of soft granular materials with free interfaces in the situations when they approach the fluid-solid transition, such as, e.g., cell aggregates, spheroids or organoids subject to external stresses. The degree to which the effect would occur may, in general, depend on the details of grain-grain and grain-interface interactions, as well as on the relation between the timescale associated with the external stresses (flow in our case) and the time scale of T1 rearrangements.

Regarding the interactions, one may expect the phenomenon to hold in homogeneous cases, with all grains being equivalent. For example, in our case, the elastic repulsive interactions can be considered homogeneous throughout the cluster. Regarding the time scales, we provide a short comparison with the work of Tlili *et al.* [19] who studied translocation of a cluster of cells through a long, narrow microchannel. The authors observed individual cell elongations, but virtually no T1 processes. The reason for that was that τ_{exp} was much smaller than τ_{T1} . In fact, the authors measured τ_{T1} in a separate long-term experiment in which only several neighboring cells were tracked, but not the whole cluster. Therefore, the dynamic effects associated with cell rearrangements, such as interior-rim separation, were not observed in the translocation experiments.

Nevertheless, in systems with homogeneous interactions and with the proper separation of time scales, we expect the reported dynamics to remain universal. In particular, our results should also translate to 3D systems and, as such, should be taken into account when considering the effective surface tension and viscosity of cell aggregates and tissues, the parameters of significant interest, e.g., in developmental biology and tissue engineering [16,47–49]. Differential deformation of cells within spheroids and embryos has been observed previously [3,50,51]. The relative role of the dynamical-topological effects in proliferating systems remains to be investigated.

At present, a comprehensive theory predicting the onset of fluidization, crystallization and effective dynamical heterogeneity in soft granular clusters, going beyond the qualitative arguments outlined above, is missing. A possible approach would encompass applying the kinetic theory of flow in soft glassy materials [52], which implies a nonlocal constitutive law for flow coupled to the rate of plastic events. Such a theory remains yet to be adapted to systems with a closed, free boundary. The type of the boundary conditions could be empirically established based on experimental results such as ours, and finally the system could be solved numerically. We leave such theoretical investigations as a future work of ours or others.

Our study opens up avenues for further experimental research. For example, the behavior of soft granular clusters at junctions or in extensional flows, resulting in stretching and breakup, remain poorly understood, and could be studied with a modified version of our system.

Finally, in terms of applications, we find that narrow orifices imposing significant elongation of a cluster can potentially serve as efficient mixers for microscale granular media. The observation could be exploited to control cell rearrangements, e.g., within cell spheroids, with potential applications in tissue and organoid engineering. Such studies could also help understand mechanical principles of tissue flow which remain of great relevance not only in tissue engineering [53], but could also shed light on the basic mechanisms of wound healing [54] and/or cancer progression including metastasis [55].

The authors acknowledge funding from the European Union's Horizon 2020 research and innovation programme under the Marie Skłodowska-Curie Grant agreement No. 847413 and from the European Research Council (ERC-PoC Grants No. 101081171 (DropTrack) and No. 101001267 (MAPEI) under the Horizon Europe research and innovation funding programme). M.B. acknowledges the PMW programme of the Minister of Science and Higher Education in the years 2020-2024 No. 5005/H2020-MSCA-COFUND/2019/2 and support from the National Science Center (Narodowe Centrum Nauki) within the Miniatura Grant No. 2022/06/X/ST3/01504. J.G. acknowledges the support from the National Science Center within Sonata Bis program under Grant No. 2019/34/E/ST8/00411. M.B., L.J., and J.G. thank P. Adamczuk for technical assistance. M.D. and S.S. thank A. Tiribocchi and M. Lauricella for fruitful discussions. We gratefully acknowledge the HPC infrastructure and the Support Team at Fondazione Istituto Italiano di Tecnologia.

M.B., S.S., G.V., and J.G. conceived and designed the study. M.B. and L.J. performed the experiments. M.B., J.P., M.D., L.J., and J.G. analyzed the data. M.B.,

J.P., M.D., and L.J. contributed materials and/or analysis tools, M.B., J.P., M.D., S.S., G.V., and J.G. wrote the manuscript.

-
- [1] K. Guevorkian, M.-J. Colbert, M. Durth, S. Dufour, and F. Brochard-Wyart, Aspiration of biological viscoelastic drops, *Phys. Rev. Lett.* **104**, 218101 (2010).
- [2] S. Douezan, K. Guevorkian, R. Naouar, S. Dufour, D. Cuvelier, and F. Brochard-Wyart, Spreading dynamics and wetting transition of cellular aggregates, *Proc. Natl. Acad. Sci. USA* **108**, 7315 (2011).
- [3] M. L. Manning, R. A. Foty, M. S. Steinberg, and E.-M. Schotz, Coaction of intercellular adhesion and cortical tension specifies tissue surface tension, *Proc. Natl. Acad. Sci. USA* **107**, 12517 (2010).
- [4] S. Cohen-Addad, R. Höhler, and O. Pitois, Flow in foams and flowing foams, *Annu. Rev. Fluid Mech.* **45**, 241 (2013).
- [5] S. Nezamabadi, T. H. Nguyen, J. Y. Delenne, and F. Radjai, Modeling soft granular materials, *Granul. Matter* **19**, 8 (2017).
- [6] A. A. J. Kabla, Collective cell migration: Leadership, invasion and segregation, *J. R. Soc. Interface* **9**, 3268 (2012).
- [7] S. Pawlizak, A. W. Fritsch, S. Grosser, D. Ahrens, T. Thalheim, S. Riedel, T. R. Kiessling, L. Oswald, M. Zink, M. L. Manning, and J. A. Käs, Testing the differential adhesion hypothesis across the epithelial-mesenchymal transition, *New J. Phys.* **17**, 083049 (2015).
- [8] Y. Jiang, P. J. Swart, A. Saxena, M. Asipauskas, and J. A. Glazier, Hysteresis and avalanches in two-dimensional foam rheology simulations, *Phys. Rev. E* **59**, 5819 (1999).
- [9] P. Marmottant and F. Graner, Plastic and viscous dissipations in foams: Cross-over from low to high shear rates, *Soft Matter* **9**, 9602 (2013).
- [10] P. Kumar, E. Korkolis, R. Benzi, D. Denisov, A. Niemeijer, P. Schall, F. Toschi, and J. Trampert, On interevent time distributions of avalanche dynamics, *Sci. Rep.* **10**, 626 (2020).
- [11] J. Goyon, A. Colin, G. Ovarlez, A. Ajdari, and L. Bocquet, Spatial cooperativity in soft glassy flows, *Nature (London)* **454**, 84 (2008).
- [12] J. Goyon, A. Colin, and L. Bocquet, How does a soft glassy material flow: Finite size effects, nonlocal rheology, and flow cooperativity, *Soft Matter* **6**, 2668 (2010).
- [13] M. Lulli, R. Benzi, and M. Sbragaglia, Metastability at the yield-stress transition in soft glasses, *Phys. Rev. X* **8**, 021031 (2018).
- [14] A. Montessori, A. Tiribocchi, M. Bogdan, F. Bonaccorso, M. Lauricella, J. Guzowski, and S. Succi, Translocation dynamics of high-internal phase double emulsions in narrow channels, *Langmuir* **37**, 9026 (2021).
- [15] P. Sollich, Rheological constitutive equation for a model of soft glassy materials, *Phys. Rev. E* **58**, 738 (1998).
- [16] R. A. Foty, G. Forgacs, C. M. Pflieger, and M. S. Steinberg, Liquid properties of embryonic tissues: Measurement of interfacial tensions, *Phys. Rev. Lett.* **72**, 2298 (1994).
- [17] E.-M. Schotz, M. Lanio, J. A. Talbot, and M. L. Manning, Glassy dynamics in three-dimensional embryonic tissues, *J. R. Soc. Interface* **10**, 20130726 (2013).
- [18] S. H. Au, B. D. Storey, J. C. Moore, Q. Tang, Y. L. Chen, S. Javid, A. F. Sarioglu, R. Sullivan, M. W. Madden, R. O'Keefe, D. A. Haber, S. Maheswaran, D. M. Langenau, S. L. Stott, and M. Toner, Clusters of circulating tumor cells traverse capillary-sized vessels, *Proc. Natl. Acad. Sci. USA* **113**, 4947 (2016).
- [19] S. L. Thili, F. Graner, and H. Delanoë-Ayari, A microfluidic platform to investigate the role of mechanical constraints on tissue reorganization, *Development* **149**, dev200774 (2022).
- [20] C. B. Highley, K. H. Song, A. C. Daly, and J. A. Burdick, Jammed microgel inks for 3D printing applications, *Adv. Sci.* **6**, 1801076 (2019).
- [21] M. Constantini, J. Guzowski, P. J. Žuk, P. Mozetic, S. De Panfilis, J. Jaroszewicz, M. Heljak, M. Massimi, M. Pierron, M. Trombetta, M. Dentini, W. Świączkowski, A. Rainer, P. Garstecki, and A. Barbeta, Electric field assisted microfluidic platform for generation of tailorable porous microbeads as cell carriers for tissue engineering, *Adv. Funct. Mater.* **28**, 1800874 (2018).
- [22] J. Guzowski, R. J. Buda, M. Costantini, M. Ćwiklińska, P. Garstecki, and H. A. Stone, From dynamic self-organization to avalanching instabilities in soft-granular threads, *Soft Matter* **18**, 1801 (2022).
- [23] J. Li and D. A. Barrow, A new droplet-forming fluidic junction for the generation of highly compartmentalised capsules, *Lab Chip* **17**, 2873 (2017).
- [24] J. Guzowski and P. Garstecki, Droplet clusters: Exploring the phase space of soft mesoscale atoms, *Phys. Rev. Lett.* **114**, 188302 (2015).
- [25] Y. K. Lai, A. S. Opalski, P. Garstecki, L. Derzsi, and J. Guzowski, A double-step emulsification device for direct generation of double emulsions, *Soft Matter* **18**, 6157 (2022).
- [26] S. Huang, S. Zeng, Z. He, and B. Lin, Water-actuated microcapsules fabricated by microfluidics, *Lab Chip* **11**, 3407 (2011).
- [27] S. H. Kim, H. Hwang, C. H. Lim, J. W. Shim, and S. M. Yang, Packing of emulsion droplets: Structural and functional motifs for multi-cored microcapsules, *Adv. Funct. Mater.* **21**, 1608 (2011).
- [28] L. L. A. Adams and S. A. Ocko, Breaking chiral symmetry with microfluidics, *arXiv:1804.07198v1*.
- [29] M. Layachi, L. Casas-Ferrer, G. Massiera, and L. Casanellas, Rheology of vesicle prototissues: A microfluidic approach, *Front. Phys.* **10**, 1045502 (2022).
- [30] C. Holtze, A. C. Rowat, J. J. Agresti, J. B. Hutchison, F. E. Angilè, C. H. Schmitz, S. Köster, H. Duan, K. J. Humphry, R. A. Scanga, J. S. Johnson, D. Pisignano, and D. A. Weitz, Biocompatible surfactants for water-in-fluorocarbon emulsions, *Lab Chip* **8**, 1632 (2008).
- [31] Y. Gai, C. M. Leong, W. Cai, and S. K. Tang, Spatiotemporal periodicity of dislocation dynamics in a two-dimensional microfluidic crystal flowing in a tapered channel, *Proc. Natl. Acad. Sci. USA* **113**, 12082 (2016).
- [32] Y. Gai, J. W. Khor, and S. K. Tang, Confinement and viscosity ratio effect on droplet break-up in a concentrated emulsion flowing through a narrow constriction, *Lab Chip* **16**, 3058 (2016).

- [33] J.-P. Raven and P. Marmottant, Microfluidic crystals: Dynamic interplay between rearrangement waves and flow, *Phys. Rev. Lett.* **102**, 084501 (2009).
- [34] P. Garstecki and G. M. Whitesides, Flowing crystals: Nonequilibrium structure of foam, *Phys. Rev. Lett.* **97**, 024503 (2006).
- [35] A. Panaitescu, K. A. Reddy, and A. Kudrolli, Nucleation and crystal growth in sheared granular sphere packings, *Phys. Rev. Lett.* **108**, 108001 (2012).
- [36] F. Rietz, C. Radin, H. L. Swinney, and M. Schröter, Nucleation in sheared granular matter, *Phys. Rev. Lett.* **120**, 055701 (2018).
- [37] A. Tiribocchi, A. Montessori, M. Lauricella, F. Bonaccorso, S. Succi, S. Aime, M. Milani, and D. A. Weitz, The vortex-driven dynamics of droplets within droplets, *Nat. Commun.* **12**, 82 (2021).
- [38] See Supplemental Material at <http://link.aps.org/supplemental/10.1103/PhysRevResearch.6.L032031> for additional details on the experimental and computational methods, data on droplet flow patterns and data on droplet circularity based on additional experiments.
- [39] M. Bogdan, A. Montessori, A. Tiribocchi, F. Bonaccorso, M. Lauricella, L. Jurkiewicz, S. Succi, and J. Guzowski, Stochastic jetting and dripping in confined soft granular flows, *Phys. Rev. Lett.* **128**, 128001 (2022).
- [40] B. Midtvedt, S. Helgadottir, A. Argun, J. Pineda, D. Midtvedt, and G. Volpe, Quantitative digital microscopy with deep learning, *Appl. Phys. Rev.* **8**, 011310 (2021).
- [41] J. Guzowski, S. Jakiela, P. M. Korczyk, and P. Garstecki, Custom tailoring multiple droplets one-by-one, *Lab Chip* **13**, 4308 (2013).
- [42] A. Montessori, A. Tiribocchi, M. Lauricella, F. Bonaccorso, and S. Succi, Mesoscale modelling of droplets' self-assembly in microfluidic channels, *Soft Matter* **17**, 2374 (2021).
- [43] P. Petit, J. Seiwert, I. Cantat, and A.-L. Biance, On the generation of a foam film during a topological rearrangement, *J. Fluid Mech.* **763**, 286 (2015).
- [44] S. J. Cox, F. Graner, M. F. Vaz, C. Monnereau-Pittet, and N. Pittet, Minimal perimeter for N identical bubbles in two dimensions: Calculations and simulations, *Philos. Mag.* **83**, 1393 (2003).
- [45] Y. Gai, A. Bick, and S. K. Y. Tang, Timescale and spatial distribution of local plastic events in a two-dimensional microfluidic crystal, *Phys. Rev. Fluids* **4**, 014201 (2019).
- [46] L. Zhu and F. Gallaire, A pancake droplet translating in a Hele-Shaw cell: Lubrication film and flow field, *J. Fluid Mech.* **798**, 955 (2016).
- [47] M. S. Steinberg, Differential adhesion in morphogenesis: A modern view, *Curr. Opin. Genet. Dev.* **17**, 281 (2007).
- [48] E. M. Schötz, R. D. Burdine, F. Jülicher, M. S. Steinberg, C. P. Heisenberg, and R. A. Foty, Quantitative differences in tissue surface tension influence zebrafish germ layer positioning, *HFSP J.* **2**, 42 (2008).
- [49] T. V. Stirbat, A. Mgharbel, S. Bodenec, K. Ferri, H. C. Mertani, J. P. Rieu, and H. Delanoë-Ayari, Fine tuning of tissues' viscosity and surface tension through contractility suggests a new role for α -catenin, *PLoS ONE* **8**, e52554 (2013).
- [50] F. Xiong, W. Ma, T. W. Hiscock, K. R. Mosaliganti, A. R. Tentner, K. A. Brakke, N. Rannou, A. Gelas, L. Souhait, I. A. Swinburne, N. D. Obholzer, and S. G. Megason, Interplay of cell shape and division orientation promotes robust morphogenesis of developing epithelia, *Cell* **159**, 415 (2014).
- [51] S. Sart, R. F. Tomasi, G. Amselem, and C. N. Baroud, Multi-scale cytometry and regulation of 3D cell cultures on a chip, *Nat. Commun.* **8**, 469 (2017).
- [52] L. Bocquet, A. Colin, and A. Ajdari, Kinetic theory of plastic flow in soft glassy materials, *Phys. Rev. Lett.* **103**, 036001 (2009).
- [53] I. Kosztin, G. Vunjak-Novakovic, and G. Forgacs, *Colloquium: Modeling the dynamics of multicellular systems: Application to tissue engineering*, *Rev. Mod. Phys.* **84**, 1791 (2012).
- [54] L. Petitjean, M. Reffay, E. Grasland-Mongrain, M. Poujade, B. Ladoux, A. Buguin, and P. Silberzan, Velocity fields in a collectively migrating epithelium, *Biophys. J.* **98**, 1790 (2010).
- [55] P. Friedl and D. Gilmour, Collective cell migration in morphogenesis, regeneration and cancer, *Nat. Rev. Mol. Cell Biol.* **10**, 445 (2009).